Available online at www.sciencedirect.com
ScienceDirect
Geochimica et Cosmochimica Acta 70 (2006) 4356–4366
Geochimica
www.elsevier.com/locate/gca

A comparative study of the effect of desferrioxamine B, oxalic acid, and Na-alginate on the desorption of U(VI) from goethite at pH 6 and 25 °C

Domenik Wolff-Boenisch *, Samuel J. Traina

Sierra Nevada Research Institute, University of California, Merced, CA 95344, USA

Received 30 January 2006; accepted in revised form 29 June 2006

Abstract

Organic ligands affect the sorption and mobility of radionuclides in soils. Batch desorption experiments on goethite particles reveal the extent of uranyl desorption and hence bioavailability with different organic acids. The desorptive strength increases in the following order: background electrolyte < Na-alginate < desferrioxamine B (DFO-B) < oxalate. The sequence is consistent with decreasing molecular size and mass from alginate via DFO-B to oxalate. The concomitant Fe release in the desorption experiments indicates that desorption from goethite and not dissolution of goethite governs the mobility of adsorbed U(VI). A compilation of DFO-B surface excesses on goethite from our experiments together with literature values indicate that DFO-B adsorbs at a constant ~3% to the goethite surface. It is surprising that such a small fraction suffices to account for the considerable uranyl desorption and thus remobilization of a radionuclide into solution. Oxalate displays higher surface concentrations but still lower than the determined uranyl surface excess. It follows that based on the high U(VI) stability constants, both organic ligands induce the desorption of uranyl species by increasing the chemical affinity of the aqueous phase. In the case of alginate, desorption of uranyl is weak and adsorbed alginate hampers any considerable detachment of U(VI) in the presence of the more potent ligands, DFO-B and oxalate. This inhibition is based on biosorption and in this respect polysaccharides in soils may retard and even halt the advance of actinides through the soil column. This hypothesis calls for further studies into the interaction of siderophores and polysaccharides with soil adsorbents and their role in the mobilization of contaminant metals.

1. Introduction

Uranium is the principal element in the processing and disposal of materials during nuclear energy and nuclear weapons production. It is also the major contaminant in soils and groundwater at sites associated with the aforementioned processes. According to MacDonald (1999), the remediation of contamination caused by the manufacturing of nuclear weapons (e.g. uranium mining) in the United States is the most monumental environmental restoration task in history. To achieve this objective a comprehensive understanding of the thermodynamics and kinetics of the physicochemical reactions occurring in the various affected environmental compartments is crucial. Especially the removal and immobilization of radionuclide contaminants in soils by microbial transformations, sorption and mineralization show the purging potential some natural and engineered microbes may have (Barkay and Schaefer, 2001). Recent studies have focused on the interaction of actinides with siderophores, a group of iron chelators which are produced by bacteria and other microbes to overcome low iron availability. Their principal function is to acquire ferric iron by dissolving poorly soluble iron minerals and oxides and mediate iron transport and deposition inside the cell (Boukhalfa and Crumbliss, 2002). Although originally synthesized as a means of sequestering ferric iron, siderophores have been shown to complex other metals and radionuclides such as Pu(IV) (Birch and Bachhofen, 1990; John et al., 2001). In the case of Pu, its complexation and subsequent uptake into the bacterial cell

* Corresponding author. Fax: +1 209 724 4424.
E-mail address: dwolff-boenisch@ucmerced.edu (D. Wolff-Boenisch).

0016-7037/$ - see front matter © 2006 Elsevier Inc. All rights reserved.
doi:10.1016/j.gca.2006.06.1565

reduces significantly the mobility of the metal and might present a future bioremediation tool in the clean-up of actinide contaminated soils (John et al., 2001). However, the same study demonstrated the lack of U(VI) uptake and hence not all actinides are sequestered or even absorbed in the same magnitude. Despite these findings, the principal biogeochemical reactions that govern the concentration, chemical speciation, and distribution of radionuclide-siderophore complexes are not fully understood and quantified and the objective of this study is to contribute to the understanding of the environmental fate of the mobile oxidized uranium in soils under the influence of the biosphere. Towards that goal U(VI) desorption experiments on goethite surfaces were performed in the presence and absence of an aliphatic siderophore, oxalic acid and the polysaccharide Na-alginate. Goethite was chosen as model soil constituent because Fe(III)oxyhydroxides are among the most reactive surfaces found in soils and goethite is the most stable Fe-oxyhydroxide. From the pool of multitudinous siderophores, desferrioxamine (DFO-B) was selected. DFO-B has three metal binding *hydroxamate* functional groups which act as bidentate ligands each. Hence, it forms a 1:1 hexadentate complex with aqueous Fe(III). Its effect on the dissolution of diverse oxides/silicates has been extensively investigated including goethite (Watteau and Berthelin, 1994; Kraemer et al., 1999; Cocozza et al., 2002; Cervini-Silva and Sposito, 2002; Cheah et al., 2003; Borer et al., 2005), hematite (Hersman et al., 1995), hornblende (Liermann et al., 2000; Kalinowski et al., 2000), biotite (Watteau and Berthelin, 1994), clay minerals (Neubauer et al., 2002; Rosenberg and Maurice, 2003) and Pu-oxide/hydroxide (Brainard et al., 1992; Ruggiero et al., 2002). Additional studies show that DFO-B not only affects the dissolution but also the sorption of metals from/to soil constituents (Kraemer et al., 1999, 2002; Neubauer and Furrer, 1999; Neubauer et al., 2000; Dubbin and Ander, 2003; Mustafa et al., 2004; Hepinstall and Maurice, 2004).

Alginate $(C_6H_8O_6)_n$, a natural polysaccharide found in brown algae, is a linear copolymer of β-D-mannuronic (M) and α-L-guluronic (G) acid residues (Haug et al., 1974). These monomers arrange themselves as polymeric M and G blocks intercalated with regions of alternating structure (MG blocks, Fig. 1). Only limited studies exist on the influence of the biofilm forming alginate-type polysaccharides on dissolution and sorption processes in the geosphere (Scharer and Byerley, 1989; Welch et al., 1999; Raize et al., 2004).

At present, there does not exist any investigation on the mobilization of U(VI) from goethite surfaces under the influence of the above-mentioned organic acids and the present study aims at filling this gap.

2. Materials and methods

Uranium-nitrate $[UO_2(NO_3)_2]$ was obtained from Lawrence Berkeley National Laboratory and the three organic acids used in this study were purchased from Sigma–Aldrich (USA). No purification grade of the desferrioxamine B mesylate salt $[C_{25}H_{46}N_5O_8NH_3^+(CH_3SO_3^-)]$ was provided by the manufacturer while oxalic acid was purified grade (99.999%). The source for the alginic acid sodium salt (low viscosity) was brown algae. No further information was available on its species origin. Goethite (α-FeOOH) was synthesized using a method described by Schwertmann and Cornell (1991). In brief, 100 mL of a 1 M $Fe(NO_3)_3$ solution was mixed with 180 mL of a 5 M KOH solution. The resulting suspension of ferrihydrite was diluted to 2 L and kept at 70 °C for 60 h to produce yellow brown goethite. Powder X-ray diffraction (XRD) confirmed that the synthesized solid was pure goethite. The XRD data were collected from 10 to 70° 2θ using a Philips XRD diffractometer equipped with a graphite-monochromatized Cu K_α X-ray source (35 kV, 20 mA). Specific surface area measurements after Brunauer et al. (1938) yielded 34.4 m^2/g and were performed using a triple point N_2 concentration adsorption isotherm on a Micromeritics Flowsorb II 2300 device.

All sorption and dissolution experiments were conducted at 25 °C, pH 6 and an ionic strength of 10 mM. The adsorbent concentration was set at 0.5 g/kg. The background electrolyte constituting every experimental solution was prepared with 18 MΩ/cm Millipore™ water and consisted of 8 mM $NaNO_3$ and a 2 mM buffer of 2-(N-morpholino)ethanesulfonic acid (MES, from Sigma). The pH was adjusted with NaOH. MES was chosen as a pH buffer because of its low metal binding constants which has been demonstrated for Mg, Ca, Mn, Cu (Good et al., 1966) and Cd, Pb (Soares et al., 1999). All sorption experiments were carried out in batch mode in acid washed 35 ml polypropylene copolymer (PPCO) high-speed centrifuging tubes

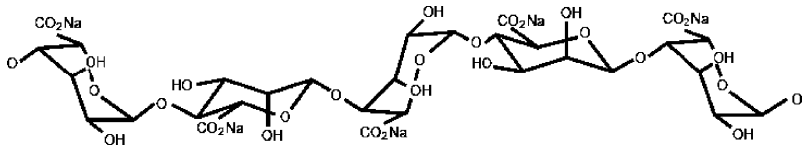

Fig. 1. The structure of alginate varies depending on the source of its formation. The principal compounds are β-D-mannuronic (M) and α-L-guluronic (G) acid residues. These monomers $(C_6H_8O_6)$ form homopolymeric MMM... and GGG... blocks and strictly alternating GMGM sequences. The latter is presented here with vertically (G) and horizontally arranged (M) molecules. Note that the main ligand (the carboxyl group) is shown saturated with Na as sodium alginate was the starting material of our alginate experiments.

from Nalgene™. The tubes were agitated for 48 h on an orbital shaker installed in an incubator at 200 rpm and 25 °C. After this contact time, samples were centrifuged at 15,000 rpm for 60 min and the supernatant quantitatively removed and filtered through a 0.2 μM nylon filter (Whatman™). Although this filter size would have allowed Fe nanoparticles to enter the solution no conspicuous Fe peaks were observed in the analyses by inductively coupled plasma mass spectrometry (ICP-MS). Since all iron—solute or suspended solid—enters the plasma the absence of such aberrantly high Fe concentrations indicates that no submicron Fe particles were present. Subsequent desorption and dissolution experiments were run immediately following the adsorption experiments. To maintain the initial solid concentration, the same mass of fresh solution was added as the mass removed after centrifugation. The new solution was then treated in the same way as the initial adsorption solution and at specific time intervals (1, 5, 15, 30 min etc.) aliquots of <3 ml were extracted and immediately filtered. The collected samples were stored in the refrigerator at 6 °C and subsequently analyzed for ^{238}U and ^{56}Fe with an Agilent 7500cs ICP-MS using internal standards.

The experimental series dedicated to the adsorption of DFO-B on uranyl treated goethite was based on total organic carbon (TOC) analysis and mass balance calculations. The TOC of a DFO-B solution was compared with the TOC of a solution of DFO-B after equilibration with uranyl adsorbed goethite and with the TOC of a solution after uranyl desorption without DFO-B as baseline. The difference in TOC was ascribed to the adsorption of DFO-B on the goethite surface and varied between 3 and 6 ppm. Analyses were performed with the high sensitivity model TOC-V_{CSH} from Shimadzu whose sensitivity reaches lower ppb level and could therefore readily quantify these differences.

Speciation and saturation calculations were performed with PHREEQC 2.8 (Parkhurst and Appelo, 1999) under the experimental conditions laid out in this paragraph. Equilibrium constants for these calculations were gathered from the literature and where needed recalculated to zero ionic strength using the software 'Ionic strength corrections using specific interaction theory', V2.0, IUPAC 2004©.

3. Results and discussion

3.1. Precipitation, speciation, and adsorption

All experiments were conducted at pH 6 because >95% of uranyl adsorbed on goethite (Hsi and Langmuir, 1985; Redden et al., 1998). At circum-neutral pH solubilities of U(VI) phases reach minima in the order of μM. Thus, adsorption experiments at such U(VI) concentrations have to take potential precipitation into account. Fig. 2 exhibits the change of saturation state of the least soluble U(VI) phases schoepite ($(UO_2)_8O_2(OH)_{12}\cdot 12\,H_2O$) and uranium-hydroxide (β-$UO_2(OH)_2$) as a function of the initial aqueous U(VI) concentration. Since all experiments were air-saturated it is assumed that no reduction of uranyl to

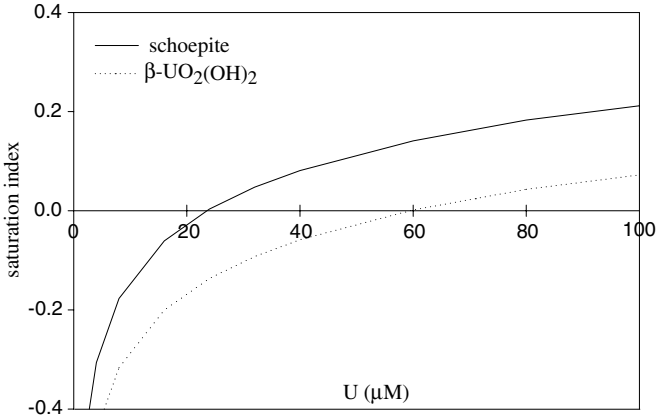

Fig. 2. Saturation state of schoepite ($(UO_2)_8O_2(OH)_{12}\cdot 12H_2O$) and uranium-hydroxide (β-$UO_2(OH)_2$) as a function of the initial uranium concentration at pH6.

U(V) or U(IV) takes place and henceforth the terms uranyl, U(VI), and uranium are used synonymously. Supersaturation with respect to the less soluble of both phases starts at 23 μM (Fig. 2) but even at 50 μM the saturation index of schoepite does not exceed 0.15. Speciation calculations and the determination of saturation indices for the two phases in question (at 50 μM initial uranyl concentration) yielded slightly positive values despite the formation of water-soluble uranyl-carbonates. However, adsorption reduces the amount of aqueous uranyl and therefore the potential for precipitation *per se*. Moreover, Giammar and Hering (2001) found that precipitation of schoepite from a U(VI)-goethite suspension at pH 6 was kinetically hindered at low degrees of supersaturation and hence in this study the highest initial employed U(VI) concentration was capped at 50 μM. The adsorption of U(VI) on goethite underlying the subsequent desorption experiments is exemplified in Fig. 3. Adsorption could be equally modeled with a Freundlich and a Langmuir isotherm as duplicate exper-

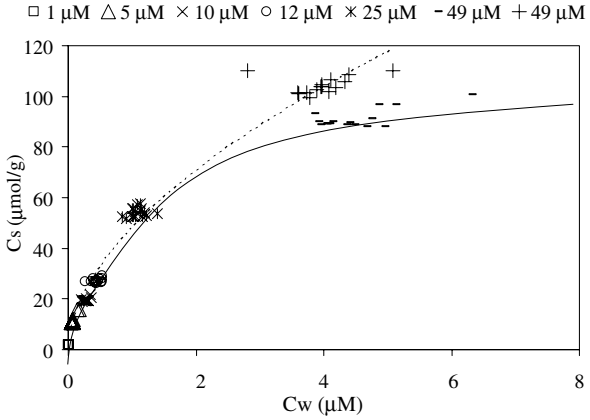

Fig. 3. Adsorption of U(VI) on goethite at pH 6 and 25 °C. The legend represents the initial U(VI) concentrations and the lines stand for a Freundlich (dashed line) and a Langmuir (solid line) fit. For the Freundlich isotherm, the parameters are: $K_F = 49.0$; $n = 0.56$. The Langmuir approach yields $K_L = 0.8\ \mu\ M^{-1}$; $\Gamma_{max} = 115$ μmol/g.

iments at the highest initial uranyl concentration (49 μM) yielded somewhat varying solid concentration values. Partition coefficients for both fits, the maximum adsorption density (Γ_{max}) and the Freundlich exponent *n* are provided in the figure caption. Γ_{max} was found to be 115 μmol/g for the Langmuir fit, in excellent agreement with a maximum adsorption density of 114 μmol/g determined under very similar experimental conditions by Giammar and Hering (2001). This value corresponds to a BET surface area normalized surface excess of uranyl of 3.3 μmol/m^2.

The limitation in the uranium concentration and the solid–solution ratio used in the present study inhibited any meaningful attempt to elucidate the surface speciation of uranium on the goethite surface in the presence/absence of the targeted ligands with either FT-IR or EXAFS. Nevertheless, potential surface species can be inferred from the work of other investigators. According to Hsi and Langmuir (1985), inner-sphere mono- and bidentate uranyl-hydroxides are the major surface species in a carbonate-free uranyl-goethite solution at neutral to alkaline pH. Under similar conditions but with CO_2 saturation Duff and Amrhein (1996) added uranyl-carbonato ternary complexes to the panoply of adsorbed species. Both studies were based exclusively on best fits of surface complexation models (SCM) and did not use surface analytical techniques to support their assumptions. Waite et al. (1994) in contrast supplemented their SCM with Extended X-ray Absorption Fine Structure (EXAFS) spectroscopy inferring an inner-sphere bidentate uranyl surface species as the sole surface complex under sub-neutral atmospheric conditions. While this was a study on ferrihydrite their conclusion was confirmed for goethite in more recent EXAFS studies (Moyes et al., 2000; Redden et al., 2001). Interestingly, Waite et al. (1994) also mentioned the appearance of a second major surface species under alkaline pH conditions. This inner-sphere bidentate uranyl-carbonato ternary surface complex was subsequently confirmed in EXAFS studies of Bargar et al. (2000) and Bostick et al. (2002). The first reference investigated uranyl-hematite adsorption while in the latter case the adsorbent was an unspecified phase of subsurface iron (hydroxides). However, the uranyl-carbonato ternary surface complex was not confined to the alkaline pH range but predominant even down to pH 4.5. Crystal truncation rod diffraction, grazing incidence EXAFS, and bond-valance calculations have also identified the presence of a binuclear, bidentate uranyl-carbonate ternary complex on hematite (Catalano et al., 2005). In contrast, *in situ* attenuated total reflection-infrared spectroscopy detected a binary, inner-sphere, multidentate surface complex of uranyl on hematite (Lefèvre et al., 2006). Remarkably, this was the only surface species detected across the pH range of 5–8. No effort was made to exclude CO_2 from the headspace or the solutions in the present study. Thus, it is assumed that the innersphere, bidentate uranyl surface complexes previously observed for hematite and ferrihydrite and indirectly assumed for goethite (Duff and Amrhein, 1996) were also present in our system.

3.2. Concentration-dependent desorption

Desorption as a function of the initial ligand concentration is presented in Fig. 4a for DFO-B. The percent ratio between the initial aqueous uranium concentration before adsorption and the recovered aqueous uranium concentration after desorption (% C_w) was introduced to account for the desorptive strength of the investigated ligands. Desorption is fast and maintains a plateau value for the duration of the reaction time. From the plateau values it is possible to infer the relationship between the DFO-B concentration and the desorptive strength (Fig. 4b). A Langmuir isotherm fits the data well suggesting a sorption model where adsorption of DFO-B on the goethite surface governs desorption of uranyl from goethite. This agrees with findings from Cheah et al. (2003) who report a Langmuir isotherm for the adsorption of DFO-B on goethite. At the same time, the Fe concentration in solution steadily increases over time (Fig. 5) indicating that dissolution of goethite takes place at uranyl-free sites. A very similar observation was made by Kraemer et al. (1999) in their study on the effect of DFO-B on Fe release and Pb(II) adsorption by goethite. Ligand-promoted dissolution was

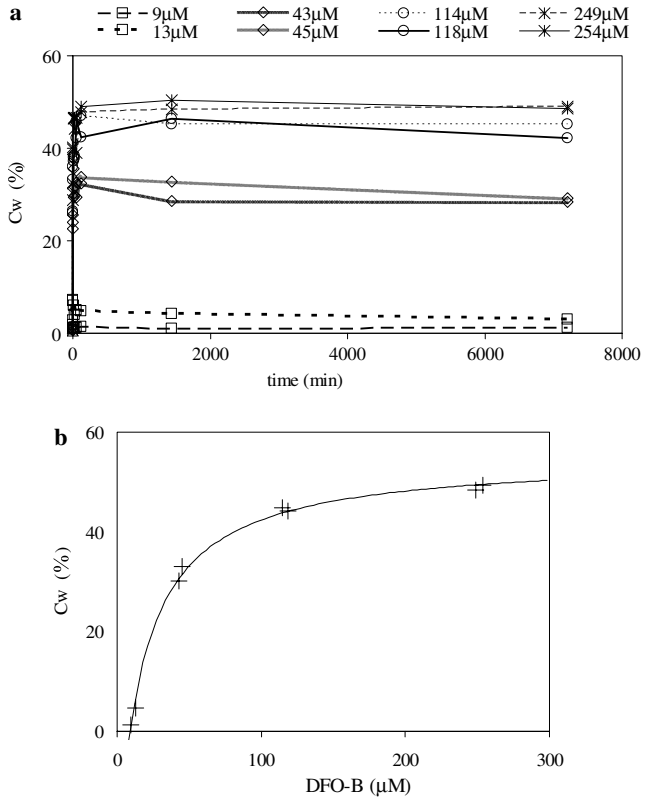

Fig. 4. (a) Desorption kinetics of uranyl (initial aqueous uranium concentration = 50 μM) from goethite as a function of the DFO-B concentration. C_w is the percent ratio between initial U concentration and recovered U concentration after desorption. (b) The constant plateau values from Fig. 4a plotted against the corresponding DFO-B concentrations. The line represents a Langmuir isotherm with $C_{w,max} = 55\%$, $K_L = 0.037\ \mu M^{-1}$.

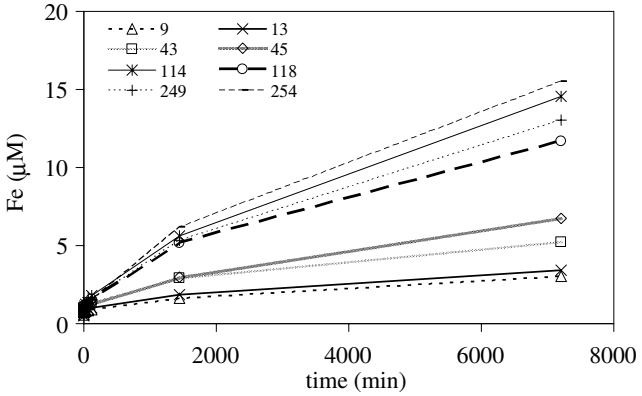

Fig. 5. Dissolution kinetics of uranyl-treated goethite at different DFO-B concentrations in μM.

unaffected by the presence of adsorbed Pb while the presence of DFO-B had a depleting effect on Pb(II) adsorption. But how do we reconcile the apparent contradiction that DFO-B promoted dissolution happens at uranyl-free sites while simultaneously DFO-B promotes desorption at U(VI) covered sites? One way is to assume different sorption and dissolution kinetics, respectively. Adsorption of cations is known to be many orders of magnitude faster than dissolution (cf. Sposito, 2004). As such, desorption of uranyl via adsorption of DFO-B can have reached equilibrium before Fe release becomes rate-controlled by a mechanism involving the (re)adsorption of excess and uncomplexed aqueous DFO-B. An alternative explanation involves the concept of indirect desorption through thermodynamic effects. The presence of aqueous DFO-B which is in excess of total uranyl and dissolved Fe leads to the quantitative complexation of these cations in solution. As a consequence, the ensuing disequilibrium between adsorbed and free aqueous U(VI) results in desorption from the surface and aqueous complexation of uranium with DFO-B until the system reaches equilibrium. As long as there is weakly bound uranium desorbing readily from goethite the successive addition of DFO-B to solution will result in further desorption. However, with increasing DFO-B concentrations, the residue of weakly bound uranium decreases and with it the fraction that desorbs from surface into solution. Finally, the more strongly complexed surface uranyl does not desorb anymore even if further ligand is added. Summarizing, increasing the chemical affinity of the system by shifting the solution position away from equilibrium also leads eventually to the Langmuir-type isotherm of Fig. 4b. In order to investigate the contribution of direct and indirect ligand-promoted desorption of uranium the desorption pattern of DFO-B is further compared to that of oxalate and alginate in the following chapter. Note that for indirect desorption to exert a considerable influence aqueous complexation of the adsorbate with the ligand must be large. To estimate indirect desorption contribution the major aqueous species under experimental conditions were modeled based on the equilibrium constants compiled in Table 1. Results of the speciation calculations are shown in Table 2. In the presence of DFO-B and oxalate, respectively, all uranium is complexed. Even prolonged goethite dissolution does not change this picture because of the excess of both ligands with respect to U and Fe. This speciation calculation indicates that all adsorbed uranium species would desorb into the DFO-B and oxalate solution if the surface bonding were not sufficiently strong to counteract this thermodynamic effect.

3.3. Ligand-dependent desorption

Desorption as a function of different ligands and initial U(VI) concentrations is presented in Fig. 6a. Two similar DFO-B concentrations (237 and 241 μM) and an equimolar amount of oxalate (242 μM) were employed. The alginate solution contained 0.5 wt% Na-alginate. Each line of each ligand in this graph represents desorption over time from a different initial uranium concentration, and the higher the initial adsorptive concentration, the higher the final recovery. The only exception is alginate where the multiple lines stand for replicates at only one initial U(VI) concentration. Consistent with Fig. 4a, desorption with DFO-B is fast and maintains comparable desorption plateau values for the duration of the reaction time. Uranium remobilization increases in the order: background electrolyte < alginate < DFO-B < oxalate. The latter reached 110% in one case reflecting analytical uncertainty in the determination of the uranium solution concentration after adsorption and desorption. Thus, the error associated with all C_w (%) values in this study is considered to be ±10%. While desorption is a very fast process for the background electrolyte and DFO-B, exhibiting both a sheave of parallel flat lines shortly after the experimental onset, oxalate and alginate display slower desorption kinetics. Desorption becomes equilibrated after 1500 min for oxalate but due to the few data points it is unclear whether or not alginate has reached a plateau after that reaction time. To illustrate how the degree of desorption varies with the initial amount of uranyl in solution, the constant C_w plateau values extracted from Fig. 6a were plotted against the initial uranium concentrations in Fig. 6b. All organic acids display a smooth enhancement in the uranyl recovery with increasing initial adsorbate concentration as more initial uranium leads to a higher surface coverage and hence more U(VI) can be subsequently desorbed.

A possible explanation for the different desorption patterns in the light of (in)direct desorption is given as follows: the organic ligand-free background electrolyte is able to 'wash off' only the loosely bound uranium (in outer-sphere or the diffuse-ion swarm), likely to be a very fast process. The lack of organic ligands advocates that the driving force for desorption is a re-equilibration of the system. Due to its large size the copolymer alginate, although equipped with numerous carboxylic functional groups, has *per se* difficulties accessing the goethite surface. The kinetics in Fig. 6a indicate that, despite this steric hindrance, alginate keeps on mobilizing uranium and this observation is consistent

Table 1
The logarithm of stability constants at zero ionic strength (log K_0) for potential aqueous reactions occurring in this study

Reactants	Product (s)	Log K_0 (25 °C)	Reference
H^+, HOx^-	H_2Ox	1.25	Martell et al. (2004)
H^+, Ox^{-2}	HOx^-	4.27	Martell et al. (2004)
Fe^{+3}, Ox^{-2}	$FeOx^+$	9.74[a]	Martell et al. (2004)
Fe^{+3}, $2Ox^{-2}$	$FeOx_2^-$	16.76[a]	Martell et al. (2004)
Fe^{+3}, $3Ox^{-2}$	$FeOx_3^{-3}$	20.54[a]	Martell et al. (2004)
Na^+, Ox^{-2}	$NaOx^-$	0.90	Martell et al. (2004)
UO_2^{+2}, HOx^-	UO_2HOx^+	3.88[a]	Martell et al. (2004)
UO_2^{+2}, $2HOx^-$	$UO_2(HOx)_2$	9.53[a]	Martell et al. (2004)
UO_2^{+2}, Ox^{-2}	UO_2Ox	7.41	Havel et al. (2002)
UO_2^{+2}, $2Ox^{-2}$	$UO_2Ox_2^{-2}$	11.80	Havel et al. (2002)
UO_2^{+2}, $3Ox^{-2}$	$UO_2Ox_3^{-4}$	13.96	Havel et al. (2002)
UO_2^{+2}, OH^-, H^+	UO_2^{+2}, H_2O	5.20	Guillaumont et al. (2003)
UO_2^{+2}, $2H^+$	UO_2^{+2}, $2H_2O$	12.15	Guillaumont et al. (2003)
$UO_2(OH)_3^-$, $3H^+$	UO_2^{+2}, $3H_2O$	20.25	Guillaumont et al. (2003)
$(OH)_4^{-2}$, $4H^+$	UO_2^{+2}, $4H_2O$	32.40	Guillaumont et al. (2003)
$(UO_2)_2OH^{+3}$, H^+	$2UO_2^{+2}$, H_2O	2.70	Guillaumont et al. (2003)
$(UO_2)_2(OH)_2^{+2}$, $2H^+$	$2UO_2^{+2}$, $2H_2O$	5.60	Guillaumont et al. (2003)
$(UO_2)(OH)_4^{+2}$, $4H^+$	$3UO_2^{+2}$, $4H_2O$	11.90	Guillaumont et al. (2003)
$(UO_2)_3(OH)_5^+$, $5H^+$	$3UO_2^{+2}$, $5H_2O$	15.50	Guillaumont et al. (2003)
$(UO_2)_3(OH)_7^-$, $7H^+$	$3UO_2^{+2}$, $7H_2O$	32.20	Guillaumont et al. (2003)
$(UO_2)_4(OH)_7^+$, $7H^+$	$4UO_2^{+2}$, $7H_2O$	21.90	Guillaumont et al. (2003)
UO_2^{+2}, Cl^-	UO_2Cl^+	0.17	Guillaumont et al. (2003)
UO_2^{+2}, $2Cl^-$	UO_2Cl_2	−1.10	Guillaumont et al. (2003)
UO_2^{+2}, NO_3^-	$UO_2NO_3^+$	0.30	Guillaumont et al. (2003)
UO_2^{+2}, CO_3^{-2}	UO_2CO_3	9.94	Guillaumont et al. (2003)
UO_2^{+2}, $2CO_3^{-2}$	$UO_2(CO_3)_2^{-2}$	16.61	Guillaumont et al. (2003)
UO_2^{+2}, $3CO_3^{-2}$	$UO_2(CO_3)_3^{-4}$	21.84	Guillaumont et al. (2003)
$3UO_2^{+2}$, $6CO_3^{-2}$	$(UO_2)_3(CO_3)_6^{-6}$	54.00	Guillaumont et al. (2003)
$2UO_2^{+2}$, CO_2, $4H_2O$	$(UO_2)_2CO_3(OH)_3^-$, $5H^+$	−19.01	Guillaumont et al. (2003)
$3UO_2^{+2}$, CO_2, $4H_2O$	$(UO_2)_3O(OH)_2(HCO_3)^+$, $5H^+$	−17.50	Guillaumont et al. (2003)
$11UO_2^{+2}$, $6CO_2$, $18H_2O$	$(UO_2)_{11}(CO_3)_6(OH)_{12}^{-2}$, $24H^+$	−72.00	Guillaumont et al. (2003)
$Dfob^{-3}$, H^+	$DfobH^{-2}$	11.48[a]	Martell et al. (2004)
$DfobH^{-2}$, H^+	$DfobH_2^-$	9.98[a]	Martell et al. (2004)
$DfobH_2^-$, H^+	$DfobH_3$	9.20[a]	Martell et al. (2004)
$DfobH_3$, H^+	$DfobH_4^+$	8.30[a]	Martell et al. (2004)
$DfobH^{-2}$, Fe^{+3}	$DfobHFe^+$	31.90[a]	Martell et al. (2004)
DfobFe, H^+	$DfobHFe^+$	10.38[a]	Martell et al. (2004)
$DfobHFe^+$, H^+	$DfobH_2Fe^{+2}$	1.00	Martell et al. (2004)
UO_2^{+2}, $DfobH^{-2}$	UO_2DfobH	23.78[a]	Czerwinski et al. (1997)
UO_2OH^+, $DfobH^{-2}$	UO_2Dfob^-, H_2O	18.40[a]	Czerwinski et al. (1997)
$UO_2(OH)_2$, $DfobH^{-2}$	$UO_2DfobOH^{-2}$, H_2O	23.43[a]	Czerwinski et al. (1997)
Mes^{-2}, H^+	$MesH^-$	6.27	Roy et al. (1997)
Mes^{-2}, Fe^{+3}	$MesFe^+$	4.70[a,b]	Anwar and Azab (2001)
Mes^{-2}, Fe^{+3}, OH^-	MesFeOH	−3.80[a,b]	Anwar and Azab (2001)

Reactants and products are presented consistent with the convention encountered in PHREEQC of describing charges and exponents. Ox^{-2} and $Dfob^{-3}$ stand for the deprotonated forms of oxalate and DFO-B, respectively.

[a] Constant was recalculated to zero ionic strength.

[b] Constant was determined for La^{+3} and adopted for Fe^{+3}.

with a rearrangement of the polymeric chains over time to better access the surface. Since there is no data on aqueous U-alginate stability constants it is not clear whether indirect desorption contributes to the increase of C_w. However, the observed slow desorption favors rather surface exchange reactions involving the organic ligand than a detachment induced by an aqueous disequilibrium. At such low recovery rates, likely still involving outer-sphere and/or less stable inner-sphere species, indirect desorption should be considerably faster.

Desorption plateaus between 40 and 60% C_w demonstrate that DFO-B mobilizes roughly half of the adsorbed U fraction. Since the relative amounts of the potentially prevalent surface complexes Fe-U(VI) and Fe-U(VI)-carbonate are unknown it cannot be determined if the 40–60% represent partial or preferential removal of one of these species. In the case of oxalate, however, all uranium is re-mobilized meaning that the inner-sphere bidentate species cannot have been desorbed quantitatively by virtue of an increase in chemical affinity. Oxalate must have replaced at least some fraction of uranyl on the goethite surface.

The higher desorptive strength of oxalate in comparison to DFO-B is supported by looking at the charges of the

Table 2
Major aqueous uranium species in % present in the background electrolyte (be) only, and with DFO-B or oxalate added to it

U(VI) (20μM)	be-U only	be-U + DFO-B	be-U + Oxalate
$(UO2)_3(OH)_5^+$	55.6	—	—
UO_2OH^+	25.1	—	—
$(UO_2)_4(OH)_7^+$	5.3	—	—
UO_2CO_3	4.7	—	—
UO_2^{+2}	4.2	—	—
$(UO_2)_2(OH)_2^{+2}$	2.5	—	—
$UO_2(OH)_2$	1.9	—	—
$(UO_2)_2CO_3(OH)_3^-$	0.7	—	—
UO_2DfobH	—	67.5	—
$UO_2DfobOH^{-2}$	—	32.5	—
$UO_2Oxalate$	—	—	17.9
$UO_2Oxalate_2^{-2}$	—	—	77.4
$UO_2Oxalate_3^{-4}$	—	—	4.6

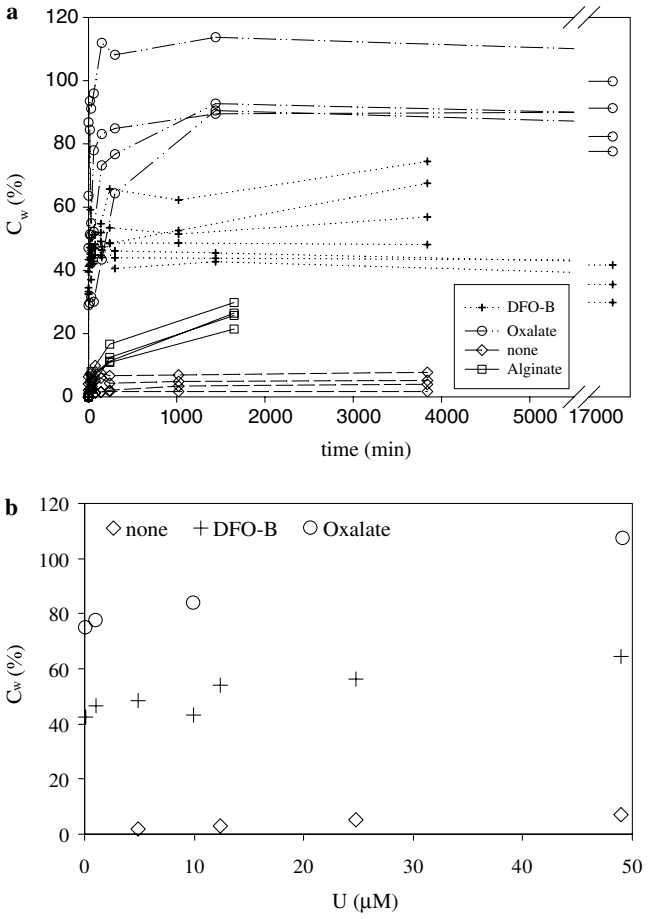

Fig. 6. (a) Desorption kinetics of uranyl surface species from goethite at pH 6 with different organic ligands. (b) The constant plateau values from Fig. 6a plotted against the initial uranyl concentrations.

principal DFO-B and oxalate species in the suspension *before* desorption (cf. Table 1). At pH 6, oxalic acid is stripped of its two protons and as doubly negatively charged $C_2O_4^{2-}$ it will readily adsorb on the positive goethite surface displacing the uranyl complexes. In contrast, the major species of DFO-B is $DfobH_4^+$, which has a positive charge like uranyl, but which is bulkier and therefore

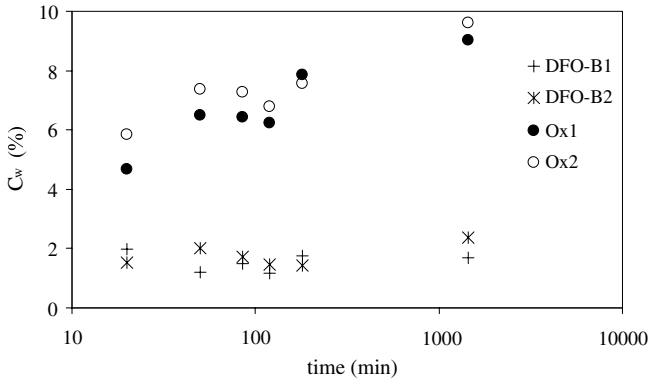

Fig. 7. Second desorption cycle of U(VI) from goethite with 240 μM of DFO-B or oxalate (Ox), in duplicate. The first desorption cycle was executed with alginate and this series constitutes a continuation of the 'Alginate' experiment displayed in Fig. 6a.

more prone to steric hindrance. As such, DFO-B should only succeed in detaching relatively weaker bonds. This assumption is consistent with results presented in Fig. 7. After uranyl desorption experiments with alginate the suspensions were phase-separated and the supernatants exchanged with 240 μM solutions of DFO-B and oxalate, in duplicate. Results of this second U(VI) desorption demonstrate that DFO-B and oxalate desorb in the same way as in Fig. 6a, i.e. rapid equilibration in the case of DFO-B and a constant increase of aqueous uranium concentration over time in the case of oxalate. DFO-B recovers only an additional 2% of the initial uranium concentration in contrast to Fig. 6a where the gap between the DFO-B and alginate desorption lines is greater. This observation hints to the presence of alginate on the goethite surface that according to Scharer and Byerley (1989) and Raize et al. (2004) sorbs and retains uranium. This potential sorption would also explain why the desorption kinetics of oxalate is slower than that in Fig. 6a as it does not reach an equilibration plateau. The fact that combined indirect and direct desorption in the presence of DFO-B yielded only another constant 2% of the initial aqueous uranium concentration indicates that all remaining uranium is strongly bound to surface iron or alginate.

Redden et al. (2001) described a citric acid promoted adsorption of uranyl on goethite—at pH $\leqslant$ 5. Fig. 6a demonstrates just the opposite, namely the ligand-promoted desorption of uranyl from goethite for a variety of organic ligands (including oxalate) at pH 6. To hold the pH change from 5 to 6 responsible for this dramatic change in the sorption behavior of uranyl is questionable because (a) the goethite surface is still far from the point of zero charge, i.e. it is still nearly as positive at pH 6 as at pH 5, and (b) citrate has the same negative charge at pH 5 as has oxalate at pH 6, thus both ligands should exhibit a similar speciating effect on uranyl. Moreover, the studies of Holmen et al. (1997) about the complexation of hydroxamate functional groups on the goethite surface indicate that identical surface complexes form at pH 3 and 6 suggesting that the

type of aHA surface complex formed does not vary significantly with pH. Redden et al. (2001) observed this ligand-promoted adsorption only at high citrate:uranyl ratios but Fig. 6b shows a smooth increase from high to low(er) ligand:uranyl ratios. It seems that the fundamental difference of both studies lies in the fact that Redden et al. (2001) let the goethite surface equilibrate with a mixed citrate-uranyl solution while in this study only uranyl was equilibrated with the goethite surface and the ligand added at a later stage. Still, the different procedures do not lend themselves to explain such opposing results as in this study the subsequent addition of the ligands could have led to a re-adsorption of a ligand-uranyl complex after desorption which was not the case. Thus it remains unclear why citrate promotes uranyl adsorption on goethite at pH $\leqslant$5 while at pH 6 oxalate (and other ligands) promote desorption of uranyl from goethite. Neubauer et al. (2002) found similar pH dependent phenomena where the percentage of dissolved Cu, Zn, and Cd in DFO-B-goethite suspensions enhanced above pH 5, 7, and 8, respectively, while below these pH values DFO-B increased the adsorption of these metals to the goethite surface. The DFO-B promoted desorption of cations from goethite at circum-neutral pH is also corroborated by other studies. Kraemer et al. (1999, 2002) postulated an adsorption inhibitory effect of DFO-B on Pb(II) and Eu^{3+} at pH $\geqslant$ 6 and Dubbin and Ander (2003) reported an increased desorption of Pb^{2+} with DFO-B at pH 6.5. A similar effect was described by Mustafa et al. (2004) with higher Cd desorption from goethite in the presence of DFO-B at pH 5.5–6. Since the pH range discussed here is at least two orders of magnitude lower than the zero point of charge of goethite ($\sim$9) or the first pK_a of DFO-B (8.3) the reason for the enhanced desorption in the presence of DFO-B cannot be found in the quasi-unaltered surface or ligand charge. This again advocates for a thermodynamic sink in solution as driving force behind desorption.

3.4. Surface excess and ligand-promoted dissolution

The finding that oxalate is a better uranyl desorbent relative to DFO-B under the experimental conditions of this study is also corroborated by Langmuir binding constants (K_L). Cheah et al. (2003) determined a K_L (at pH 5) for oxalate and DFO-B of 0.12 μM^{-1} and 0.27 μM^{-1}, respectively, compared to a K_L for uranyl of 0.8 μM^{-1} (Fig. 3). Based on these binding constants, oxalate should displace double as much uranyl from the goethite surface as DFO-B. Although this supposition is close to actual observations K_L present sorption 'affinities'. Since they do not provide any indication of the actual sorption/desorption mechanism caution should be applied in their utility. More compelling than qualitative K_L are measurable surface excesses. Djafer et al. (1991) reported 500 nmol/m^2 for oxalate adsorbed on goethite at pH 6 and an oxalate concentration of 300 μM while Cocozza et al. (2002) found a surface excess six times lower for DFO-B. Their value of 85 nmol/m^2 was again determined at a DFO-B concentration of 300 μM but at a slightly higher pH of 6.5. Own attempts to determine the DFO-B surface excess on uranyl-covered goethite were based on mass balance calculations of total organic carbon measurements as described above. Fig. 8 illustrates triplicate TOC measurements at four different initial uranium concentrations that were recalculated to the amount of DFO-B attached to the surface. As expected with this kind of experimental approach there is certain overall scatter but the triplicate determinations are reasonably good. The confidence interval for the linear regression clearly indicates that no trend between aqueous uranium and adsorbed DFO-B concentration can be inferred from this graph. Whether this lack of trend is a consequence of the very low goethite and initial U(VI) concentrations or because DFO-B adsorption takes place at uranyl-free sites anyway can not be answered conclusively. In comparison to the value provided by Cocozza et al. (2002), this TOC experiment yields an average of 226 nmol/m^2, 2.7 times higher. Curiously, the initial DFO-B concentration in this case was 109 μM, 2.7 times lower. Based on this observation, DFO-B and oxalate surface excess literature values on goethite at sub-neutral pH were collected and Fig. 9 prepared. Data points of this comparative study and parameters required for its calculation are presented in Table 3. To avoid any potential solid concentration effect on the ligand adsorption which may occur at such diverse solid concentrations ranging from 0.5 to 20 g/kg the aqueous ligand concentration was normalized to the goethite concentration of the respective study. This measure is backed by the disappearance of the relationship in Fig. 9 when plotting the ligand surface concentration against the aqueous ligand concentration (not shown). The open symbols represent oxalate data while all other symbols stand for DFO-B surface excesses.

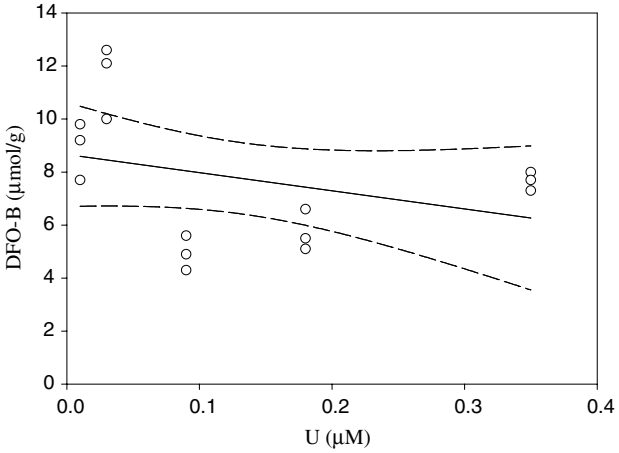

Fig. 8. DFO-B surface concentrations (open circles) as a function of the initial aqueous uranium concentrations based on triplicate TOC determinations. The solid line represents a linear fit through all the data and the dashed lines stand for the 95% confidence interval. The mean is 7.8 ± 2.6 μmol/g adsorbed DFO-B.

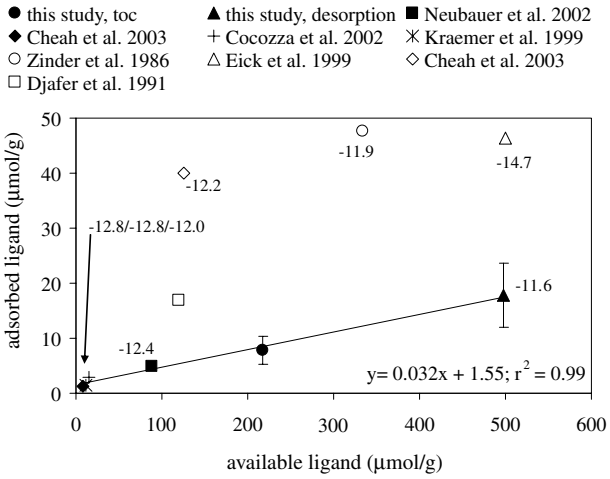

Fig. 9. Aqueous ligand concentrations normalized to the suspension load yielding the theoretically maximum ligand saturation on goethite. This parameter was compared to the amount of ligand that effectively adsorbed. The black symbols, the cross and the star represent DFO-B adsorption data through which a linear regression was laid. The slope of this linear fit corresponds to the adsorbed fraction ($3.2 \pm 1.2\%$). The open symbols originate from oxalate adsorption studies and the numbers added stand for ligand-promoted goethite dissolution rates in mol/m^2/s. Table 3 compiles the pertinent data underlying this graph.

The ligand surface excess of the black triangle was not determined experimentally as in the case of all the other data points. It was derived assuming that the surface excess percentage determined from the TOC experiment (3.6%) together with its associated error is applicable to the desorption experiments that were executed under the same experimental set-up but at higher initial DFO-B concentrations of 249 μM (cf. Table 3). The error bars reflect the scatter in Fig. 8. Still, the linear relationship between the maximum theoretically adsorbable DFO-B solid concentration and the real adsorbed concentration is evident. To this relationship were added the ligand-promoted goethite dissolution rates, where available. Except for one value these rates follow the trend of increasing DFO-B promoted dissolution rates with increasing DFO-B surface excess. This observation matches the findings of Cervini-Silva and Sposito (2002) and Cheah et al. (2003) reporting proportionality between the goethite dissolution rate and the DFO-B surface excess. Such an observation does not necessarily favor direct over indirect desorption as the absolute adsorbate surface concentration and the aqueous chemical affinity increase in both cases. In the case of oxalate, three of the four available data points have very similar adsorbed ligand concentrations. Since these values correspond to high oxalate concentrations $\geqslant 1000$ μM (cf. Table 3) they indicate saturation of the surface sites with this ligand. The fourth point in contrast corresponds to an aqueous oxalate concentration of 300 μM and has not reached solid saturation yet. Two of the three available oxalate-promoted dissolution rates are similar and thus consistent with the explanation above.

4. Conclusions

The desorptive strength of the three ligands enhances in the following order: alginate < DFO-B < oxalate. The concomitant Fe release in the desorption experiments demonstrates that (in)direct desorption from goethite and not dissolution of goethite governs the mobility of adsorbed U(VI) at pH 6 for all three ligands (data only shown for DFO-B). The sequence is consistent with decreasing molecular size and mass from alginate via DFO-B to oxalate and therefore suggests the contribution of steric hindrance or stereochemical effects to the desorption process. This proposition is corroborated by a comparison of DFO-B surface excesses of our experimental data with literature values. Normalized to the adsorbent concentration the compilation reveals that DFO-B adsorbs only $3.2 \pm 1.2\%$ to the goethite surface. This intriguingly small fraction corresponds to a surface excess of 8 μmol/g (Table 3) in contrast to a uranyl surface excess of 115 μmol/g (Fig. 3). Therefore, the mobilization of roughly half of adsorbed uranium (cf. Fig. 4b) indicates the contribution from indirect desorption, i.e. uranyl desorption mediated by disequilibrium in solution. For oxalate, desorption of U(VI) is quantitative and therefore requires active and direct detachment of the energetically most stable uranium surface species. Persson and Axe (2005) determined the ratio between outer-sphere and inner-sphere oxalate species on pure goethite as a function of pH and total oxalate concen-

Table 3
Compilation of experimental parameters and results referring to Fig. 9

References	pH	BET (m^2/g)	Goethite (g/L μM)	DFO-B	Total ligand (μmol/g)	Surf. excess (μmol/g)	Surf. excess (μmol/m^2)
Cheah et al. (2003)	5	35	10	80	8	1.2	0.034
Cocozza et al. (2002)	6.5	35	20	300	15	2.99	0.085
Kraemer et al. (1999)	6.6	35	13	150	11.5	1.5	0.043
Neubauer et al. (2002)	6	21	1	88	88	5	0.238
This study, toc	6	34.4	0.5	109	218	7.8	0.226
This study, desorption	6	34.4	0.5	249	498	17.8	0.516
Oxalate							
Zinder et al. (1986)	6	19	3	1000	333	48	2.51
Eick et al. (1999)	6	55.5	10	5000	500	46	0.83
Cheah et al. (2003)	5	35	10	1250	125	40	1.14
Djafer et al. (1991)	6	34	2.5	300	120	17	0.50

tration. Extrapolating their findings to our experimental conditions at ten times higher oxalate concentration yields a value of at least 0.5, i.e. half as many outer-sphere than inner-sphere complexes. The question arises whether the inner-sphere portion of oxalate is sufficient to remove all (principally bidentate bonded) adsorbed U(VI) or whether the outer-sphere fraction contributes to this detachment. In the lower part of Table 3 the surface excesses of oxalate on goethite at different initial oxalate concentrations from the literature are compiled. The value of 17 μmol/g from Djafer et al. (1991) comes closest to our experimental conditions. As in the case of DFO-B, this surface concentration is considerably lower than the determined uranium surface concentration. To account for the quantitative desorption some surface-complexed uranium must have been detached through indirect desorption. The ratio between direct and indirect desorption cannot be quantified. Qualitatively, it appears as if both mechanisms were comparable in magnitude. In the case of DFO-B the contribution from direct desorption based on the discrepancy of surface excesses seems negligible. Assuming then that 55% of desorbed uranium is probably due to indirect desorption (Fig. 4b) it leaves 45% (52 μmol/g) of surface-complexed U(VI). This hypothetical value is still three times higher than the oxalate surface excess of 17 μmol/g from Djafer et al. (1991) but it comes close to the oxalate surface saturation values given by the other references (cf. Table 3). Ruling out the contribution of outer-sphere oxalate-goethite species in the displacement of inner-sphere bidentate U(VI) complexes would only exacerbate the observed discrepancy by another 1/3. It should be emphasized that these conclusions are based on the comparison of surface excesses determined in separate systems. Whether surface excesses of different ligands in general or discrepancies between them are indeed indicative of the portion of (in)direct desorption has not been established in the scientific literature and the discussion presented here is meant as a starting point for future studies on this issue.

Oxalate provokes a nearly quantitative mobilization of uranium but its subsequent aqueous complexation (cf. Table 2) yields mainly $UO_2Oxalate_2^{2-}$, a doubly negatively charged species more likely to re-adsorb on positively charged adsorbents than the original singly positively charged U(VI) species themselves. In contrast, DFO-B desorbs 'only' ~55% from the original uranium concentration but the complexation results principally in a stable neutral species not probable to re-adsorb in great quantities. Hence, the ligand-effect on the bioavailability of U(VI) is not only restricted to its desorptive strength but also encompasses the aqueous speciation that follows desorption. Concerning alginate, it appears to actively desorb weakly bonded uranium. Its more important role in the bioavailability of uranium however lies it its ability to form surface species with uranium that inhibit further desorption with more potent ligands. In this respect polysaccharides in soils may retard considerably and even arrest the advance of actinides through the soil column and may therefore be an efficient tool in natural attenuation.

Acknowledgments

This manuscript greatly benefited from the insightful comments of the AE and three anonymous reviewers. The authors thank the Department of Energy for its financial support under the contract number DE-FG0204ER63762 (DOE-NABIR).

Associate editor: Garrison Sposito

References

Anwar, Z.M., Azab, H.A., 2001. Ternary complexes formed by trivalent lanthanide ions, nucleotides, and biological buffers. *J. Chem. Eng. Data* **46**, 613–618.

Bargar, J.R., Reitmeyer, R., Lenhart, J.J., Davis, J.A., 2000. Characterization of U(VI)-carbonato ternary complexes on hematite: EXAFS and electrophoretic mobility measurements. *Geochim. Cosmochim. Acta* **64**, 2737–2749.

Barkay, T., Schaefer, J., 2001. Metal and radionuclide bioremediation: issues, considerations and potentials. *Curr. Opin. Microbiol.* **4**, 318–323.

Birch, L., Bachhofen, R., 1990. Complexing agents form microorganisms. *Experientia* **46**, 827–834.

Borer, P.M., Sulzberger, B., Reichard, P., Kraemer, S.M., 2005. Effect of siderophores on the light-induced dissolution of colloidal iron(III) (hydr)oxides. *Mar. Chem.* **93**, 179–193.

Bostick, B.C., Fendorf, S., Barnett, M.O., Jardine, P.M., Brooks, S.C., 2002. Uranyl surface complexes formed on subsurface media from DOE Facilities. *Soil Sci. Soc. Am. J.* **66**, 99–108.

Boukhalfa, H., Crumbliss, A.L., 2002. Chemical aspects of siderophore mediated iron transport. *Biometals* **15**, 325–339.

Brainard, J.R., Strietelmeier, B.A., Smith, P.H., Langston-Unkefer, P.J., Barr, M.E., Ryan, R.R., 1992. Actinide binding and solubilization by microbial siderophores. *Radiochim. Acta* **58/59**, 357–363.

Brunauer, S., Emmet, P.H., Teller, E., 1938. Adsorption of gases in multimolecular layers. *J. Am. Chem. Soc.* **60**, 309–319.

Catalano, J.G., Trainor, T.P., Eng, P.J., Waychunas, G.A., Brown Jr., G.E., 2005. CTR diffraction and grazing-incidence EXAFS study of U(VI) adsorption onto α-Al_2O_3 and α-Fe_2O_3 (1102) surfaces. *Geochim. Cosmochim. Acta* **69**, 3555–3572.

Cervini-Silva, J., Sposito, G., 2002. Steady-state dissolution kinetics of aluminum-goethite in the presence of desferrioxamine-B and oxalate ligands. *Environ. Sci. Technol.* **36**, 337–342.

Cheah, S.-F., Kraemer, S.M., Cervini-Silva, J., Sposito, G., 2003. Steady-state dissolution kinetics of goethite in the presence of desferrioxamine B and oxalate ligands: implications for the microbial acquisition of iron. *Chem. Geol.* **198**, 63–75.

Cocozza, C., Tsao, C.C.G., Cheah, S.-F., Kraemer, S.M., Raymond, K.N., Miano, T.M., Sposito, G., 2002. Temperature dependence of goethite dissolution promoted by trihydroxamate siderophores. *Geochim. Cosmochim. Acta* **66**, 431–438.

Czerwinski, K., Denecke, M.A., Pompe, S., Moll, H., Reich, T., Nitsche, H. 1997. Complexation of uranium(VI) with the siderophore desferrioxamine B. Sixth international conference on the chemistry and migration behaviour of actinides and fission products in the geosphere, October 26th–31st 1997, Sendai, Japan.

Djafer, M., Khandal, R.K., Terce, M., 1991. Interactions between different anions and the goethite surface as seen by different methods. *Colloid Surfaces* **54**, 209–218.

Dubbin, W.E., Ander, E.L., 2003. Influence of microbial hydroxamate siderophores on Pb(II) desorption from α-FeOOH. *Appl. Geochem.* **18**, 1751–1756.

Duff, M.C., Amrhein, C., 1996. Uranium(VI) adsorption on goethite and soil in carbonate solutions. *Soil Sci. Soc. Am.* **60**, 1393–1400.

Eick, M.J., Peak, J.D., Brady, W.D., 1999. The effect of oxyanions on the oxalate-promoted dissolution of goethite. *Soil Sci. Soc. Am.* **63**, 1133–1144.

Giammar, D.E., Hering, J.G., 2001. Time scale for sorption-desorption and surface precipitation of uranyl on goethite. *Environ. Sci. Technol.* **35**, 3332–3337.

Good, N.E., Winget, D.G., Winter, W., Connolly, T.N., Izawa, S., Singh, R.M.M., 1966. Hydrogen ion buffers for biological research. *Biochemistry* **5**, 467–477.

Guillaumont, R., Fanghänel, T., Fuger, J., Grenthe, I., Neck, V., Palmer, D.A., Rand, M.H., 2003. *Update on the Chemical Thermodynamics of Uranium, Neptunium, Plutonium, Americium and Technetium*. Elsevier, Amsterdam.

Haug, A., Larsen, B., Smidsrød, O., 1974. Uronic acid sequence in alginate from different sources. *Carbohyd. Res.* **32**, 217–225.

Havel, J., Soto-Guerrero, J., Lubal, P., 2002. Spectrophotometric study of uranyl–oxalate complexation in solution. *Polyhedron* **21**, 1411–1420.

Hepinstall, S.E., Maurice, P.A. 2004. The effects of siderophores on Cd adsorption to kaolinite. Proceedings of the 11th International Symposium on Water-Rock Interaction, June 27th-July 2nd 2004, Saratoga Springs, NY, pp. 1131–1134.

Hersman, L., Lloyd, T., Sposito, G., 1995. Siderophore-promoted dissolution of hematite. *Geochim. Cosmochim. Acta* **59**, 3327–3330.

Holmen, B.A., Tejedor, M.I., Casey, W.H., 1997. Hydroxamate complexes in solution and at the goethite-water interface: A cylindrical internal reflection Fourier transform infrared spectroscopy study. *Langmuir* **13**, 2197–2206.

Hsi, C.-K.D., Langmuir, D., 1985. Adsorption of uranyl onto ferric oxyhydroxides: application of the surface complexation site-binding model. *Geochim. Cosmochim. Acta* **49**, 1931–1941.

John, S.G., Ruggiero, C.E., Hersman, L.E., Tung, C.-S., Neu, M.P., 2001. Siderophore mediated plutonium accumulation by Microbacterium flavescens (JG-9). *Environ. Sci. Technol.* **35**, 2942–2948.

Kalinowski, B.E., Liermann, L.J., Givens, S., Brantley, S.L., 2000. Rates of bacteria-promoted solubilization of Fe from minerals: a review of problems and approaches. *Chem. Geol.* **169**, 357–370.

Kraemer, S.M., Cheah, S.-F., Zapf, R., Xu, J.D., Raymond, K.N., Sposito, G., 1999. Effect of hydroxamate siderophores on Fe release and Pb(II) adsorption by goethite. *Geochim. Cosmochim. Acta* **63**, 3003–3008.

Kraemer, S.M., Xu, J.D., Raymond, K.N., Sposito, G., 2002. Adsorption of Pb(II) and Eu(III) by oxide minerals in the presence of natural and synthetic hydroxamate siderophores. *Environ. Sci. Technol.* **36**, 1287–1291.

Lefèvre, G., Noinville, S., Fédoroff, M., 2006. Study of uranyl sorption onto hematite by in situ attenuated total reflection-infrared spectroscopy. *J. Colloid Interf. Sci.* **296**, 608–613.

Liermann, L.J., Kalinowski, B.E., Brantley, S.L., Ferry, J.G., 2000. Role of bacterial siderophores in dissolution of hornblende. *Geochim. Cosmochim. Acta* **64**, 587–602.

MacDonald, J.A., 1999. Cleaning up the nuclear weapons. *Environ. Sci. Technol.* **33**, 314–319.

Martell, A.E., Smith, R.M., Motekaitis, R.J. 2004. NIST CRITICALLY SELECTED STABILITY CONSTANTS, STANDARD REFERENCE DATABASE 46, VERSION 8.0.

Moyes, L.N., Parkman, R.H., Charnock, J.M., Vaughan, D.J., Livens, F.R., Hughes, C.R., Braithwaite, A., 2000. Uranium uptake from aqueous solution by interaction with goethite, lepidocrocite, muscovite, and mackinawite: an X-ray absorption spectroscopy study. *Environ. Sci. Technol.* **34**, 1062–1068.

Mustafa, G., Singh, B., Kookana, R. 2004. Factors affecting the desorption of cadmium from goethite. Abstracts from the 41st Annual Meeting of the Clay Minerals Society, June 19th-24th 2004, Richland, Washington.

Neubauer, U., Furrer, G., 1999. The use of voltammetry for sorption studies of heavy metals on mineral surfaces in presence of the siderophore desferrioxamine B. *Anal Chim. Acta* **392**, 159–173.

Neubauer, U., Nowack, B., Furrer, G., Schulin, R., 2000. Heavy metal sorption on clay minerals affected by the siderophore desferrioxamine B. *Environ. Sci. Technol.* **34**, 2749–2755.

Neubauer, U., Furrer, G., Schulin, R., 2002. Heavy metal sorption on soil minerals affected by the siderophore desferrioxamine B: the role of Fe(III) (hydr)oxides and dissolved Fe(III). *Eur. J. Soil Sci.* **53**, 45–55.

Parkhurst D.L. and Appelo C.A.J. 1999. User's guide to PHREEQC (Version 2)-A computer program for speciation, batch-reaction, one-dimensional transport, and inverse geochemical calculations. U.S. Geol. Surv. Water Resour. Inv. Report 99–4259.

Persson, P., Axe, K., 2005. Adsorption of oxalate and malonate at the water-goethite interface: molecular surface speciation from IR spectroscopy. *Geochim. Cosmochim. Acta* **69**, 541–552.

Raize, O., Argaman, Y., Yannai, S., 2004. Mechanisms of biosorption of different heavy metals by brown marine macroalgae. *Biotechnol. Bioeng.* **87**, 451–458.

Redden, G.R., Li, J., Leckie, J., 1998. Adsorption of U(VI) and citric acid on goethite, gibbsite, and kaolinite: Comparing results for binary and ternary systems. In: Jenne, E.A. (Ed.), *Adsorption of Metals by Geomedia*. Academic Press, pp. 291–315.

Redden, G., Bargar, J., Bencheikh-Latmani, R., 2001. Citrate enhanced uranyl adsorption on goethite: an EXAFS analysis. *J. Colloid Interf. Sci.* **244**, 211–219.

Rosenberg, D.R., Maurice, P.A., 2003. Siderophore adsorption to and dissolution of kaolinite at pH 3 to 7 and 22. *Geochim. Cosmochim. Acta* **67**, 223–229.

Roy, R.N., Moore, C.P., Carlsten, J.A., Good, W.S., Harris, P., Rook, J.M., Roy, L.N., Kuhler, K.M., 1997. Second dissociation constant of two substituted amino-methanesulfonic acids in water from 5 to 55 °C. *J. Sol. Chem.* **26**, 1209–1216.

Ruggiero, C.E., Matonic, J.H., Reilly, S.D., Neu, M.P., 2002. Dissolution of plutonium(IV) hydroxide by desferrioxamine siderophores and simple organic chelators. *Inorg. Chem.* **41**, 3593–3595.

Scharer, J.M., Byerley, J.J., 1989. Aspects of uranium adsorption by microorganisms. *Hydrometallurgy* **21**, 319–329.

Schwertmann, U., Cornell, R.M., 1991. *Iron oxides in the laboratory*. VCH Publ.,, New York.

Soares, H.M.V.M., Conde, P.C.F.L., Almeida, A.A.N., Vasconcelos, M.T.S.D., 1999. Evaluation of n-substituted aminosulfonic acid pH buffers with a morpholinic ring for cadmium and lead speciation studies by electroanalytical techniques. *Anal. Chim. Acta* **394**, 325–335.

Sposito, G., 2004. *The surface chemistry of natural particles*. Oxford University Press, New York.

Waite, T.D., Davis, J.A., Payne, T.E., Waychunas, G.A., Xu, N., 1994. Uranium(VI) adsorption to ferrihydrite: application of a surface complexation model. *Geochim. Cosmochim. Acta* **58**, 5465–5478.

Watteau, F., Berthelin, J., 1994. Microbial dissolution of iron and aluminum from soil minerals—efficiency and specificity of hydroxamate siderophores compared to aliphatic acids. *Eur. J. Soil Biol.* **30**, 1–9.

Welch, S.A., Barker, W.W., Banfield, J.F., 1999. Microbial extracellular polysaccharides and plagioclase dissolution. *Geochim. Cosmochim. Acta* **63**, 1405–1419.

Zinder, B., Furrer, G., Stumm, W., 1986. The coordination chemistry of weathering: II Dissolution of Fe(III) oxides.. *Geochim. Cosmochim. Acta* **50**, 1861–1869.